Acta Geophysica (2018) 66:121–130
https://doi.org/10.1007/s11600-018-0112-7

RESEARCH ARTICLE - SOLID EARTH SCIENCES

# Simulation of the microtremor H/V spectrum based on the theory of surface wave propagation in a layered half-space

Zhen Zhang[1] · Xueliang Chen[1] · Mengtan Gao[1] · Zongchao Li[1] · Qianfeng Li[2]

Received: 17 July 2017 / Accepted: 17 January 2018 / Published online: 29 January 2018


**Abstract**
Subsurface velocity structures must be estimated to predict long-period ground motions and seismic hazards. Subsurface velocity structures can be constructed via an inversion of the horizontal-to-vertical (H/V) spectral ratio of microtremor (MHV) curves; thus, a method of simulating the MHV curves is key. In this study, we use the H/V spectral ratio of the surface wave (SHV) based on the surface wave propagation theory in a layered half-space to simulate the MHV curves at sites A and B of the Yuxi basin. Then, we attempt to analyze the features of the SHV curves. We find the H/V ratio of the microtremor loading source to be independent of the peak frequency of the SHV curve, but it has some relation to the amplitude of the SHV curve. Moreover, to reduce the error in subsurface velocity structures obtained by the MHV curves, we suggest that the SHV curves at near-peak frequencies should not be considered in the inversion, because the amplitude deviation is higher at the peak frequency of the MHV curve. In addition, the best frequency ranges for the inversion of the microtremor H/V spectrum are between the peak and trough frequencies of the microtremor H/V spectrum.

**Keywords** Seismic hazard · Velocity structure · Microtremor · Surface wave H/V spectrum · Microtremor loading source

## Introduction

After the 1985 Mexico City earthquake, scientists realized that sedimentary layers amplify the amplitude and duration of long-period ground motions (Komatitsch et al. 2004; Shani-Kadmiel et al. 2012; Rong et al. 2016). Thus, the three-dimensional (3-D) velocity structures of the subsurface sedimentary layers must be estimated for the prediction of long-period ground motions (Gao et al. 2002; Chen et al. 2014).

Subsurface shallow velocity profiles can be determined from geotechnical or geophysical investigations. Compared with data obtained by drilling and seismic exploration, microtremor data are obtained by inexpensive techniques that do not require high logistical effort (Picozzi et al. 2005). Since the 1930s, Japanese scholars have been studying microtremors. To date, the methods of estimating subsurface velocity structures from microtremor array records have mainly fallen into two categories: (1) spatial autocorrelation analysis, which was initiated by Aki (1957) and (2) frequency-wavenumber spectral analysis, which was initiated by Capon (1969). Many studies have shown that the spatial autocorrelation analysis (Apostolidis et al. 2004; Claprood et al. 2011) and frequency-wavenumber spectral analysis (Satoh et al. 2001; Wu and Huang 2012) methods were effective for evaluating the subsurface S-wave velocity structures at different sites. However, since Nogoshi and Igarashi (1971) proposed the ratio between the Fourier spectral amplitudes of the horizontal and vertical components of microtremor recordings (MHV), the horizontal-to-vertical (H/V) curves of microtremors have become a common method for evaluation of the site effect (Bonnefoy-Claudet et al. 2006; Carcione et al. 2017). In addition, the H/V curves of microtremors have been widely used to evaluate subsurface velocity structures (Delgado et al. 2000; Dolenc 2005; Hobiger et al. 2009; Özalaybey et al. 2011). Studies have also evaluated subsurface S-wave velocity structures via joint inversions of the phase velocity dispersion and H/V ratio

✉ Xueliang Chen
chenxl@cea-igp.ac.cn

[1] Institute of Geophysics, China Earthquake Administration, Beijing, China

[2] General Construction Company of CCTEB Group Co., Ltd., Wuhan, China

curves from microtremor recordings (Arai and Tokimatsu 2005; Picozzi et al. 2005).

The key to estimating subsurface velocity structures by the inversion of MHV curves is the simulation of MHV curves. At present, many methods are used to simulate MHV curves (Lunedei and Malischewsky 2015). MHV curves can be reproduced by the finite-differential method (FDM) in a 3-D soil model (Rhie and Dreger 2009), although Guéguen et al. (2007) found that the fundamental peak frequency (HVfp) of the MHV curve based on the FDM does not conform to the peak frequency (RHVfp) of the fundamental-mode Rayleigh wave H/V spectrum in areas, where irregular subsurface structures occur. Moreover, Uebayashi et al. (2012) indicated that the HVfp in a 3-D velocity model always is higher than the RHVfp. The MHV peak shape broadens in areas with irregular subsurface structures (Uebayashi 2003).

In addition, since Harkrider (1964, 1970) proposed the theory of surface wave propagation in a 1-D layered half-space, the H/V spectra of the fundamental-mode Rayleigh waves have been used to simulate the MHV curves in 1-D velocity structures (Fäh et al. 2003). The peak frequencies of the H/V spectral ratio of fundamental-mode Rayleigh waves are similar to those of the microtremors at a given site (Lachetl and Bard 1994), and Malischewsky and Scherbaum (2004) found that higher similarity corresponded to a higher impedance contrast between the layer and the half-space. However, the amplitudes are dissimilar (Yamanaka et al. 1994), because higher mode Rayleigh waves, Love waves, and body waves are observed in microtremors. The subsurface S-wave velocity structures can be successfully evaluated by the inversion of the dispersion curves of microtremor vertical motions, which indicates that microtremors mainly consist of surface waves (Horike 1985). Moreover, because body waves attenuate more rapidly than surface waves, surface waves can predominate at distances greater than one wavelength of a Rayleigh or Love wave from the source (Tamura 1996). Hence, a more reasonable approach is to simulate MHV curves using surface waves rather than body waves. On the other hand, Malischewsky and Scherbaum (2004) studied the Love formula and H/V ratio (ellipticity) of Rayleigh waves, and found that the dependence of the ellipticity of Rayleigh wave on frequency is very sensitive on the material properties of the propagation medium. Bonnefoy-Claudet et al. (2008) found that the relative proportion of Love and Rayleigh waves in microtremors depends on the site conditions (the subsurface structure and the sources may have effects on the Love wave contribution) and especially on the impedance contrast. Certain sites present a low impedance contrast when Love waves dominate the wavefield at the H/V peak (Endrun 2011).

Studies have also focused on simulating Rayleigh and Love waves (Bonnefoy-Claudet et al. 2008; Endrun 2011). Arai and Tokimatsu (2004) proposed the H/V spectral ratio of the surface wave (SHV) curves of all modes of surface waves. The Rayleigh-to-Love wave amplitude ratio (*R/L*) in the horizontal components of microtremors is important for calculating the SHV. The *R/L* values can be estimated by analyzing the spatial autocorrelation function of the microtremor array records (Köhler et al. 2006, 2007; Bonnefoy-Claudet et al. 2008). The *R/L* value varies widely (from 10 to 90%) with the frequency (Köhler et al. 2007; Endrun 2011). Arai and Tokimatsu (2000) indicated that the *R/L* values occur in a range from 0.4 to 1.0 with changes in the sites and frequencies. However, the *R/L* values are assumed to be constant at all frequencies in the inversion of the microtremor H/V spectrum, because the *R/L* values cannot be evaluated by a single-station three-component seismometer if the subsurface seismic velocity model is unknown (Arai and Tokimatsu 2000).

Moreover, based on the model for the formalization of the full wavefield, Lunedei and Albarello (2010) indicated that the numerical approximation model consisting of the surface waves is appropriate if a source-free area with a radius of suitable length occurs around the receiver. Furthermore, based on the diffuse field theory (García-Jerez et al. 2013), the MHV can be simulated as the ratio of the imaginary parts of Green's function for the horizontal components to the vertical component when the exciting and receiving points coexist on the ground surface (Sánchez-Sesma et al. 2011). In addition, the inversion result of the H/V spectral ratio under the diffuse field assumption is reproduced well (García-Jerez et al. 2016; Piña-Flores et al. 2017).

In this study, the area studied is located in the Yuxi basin in Yuxi City of southwestern China, for which high-quality drilling data have been obtained and a precise subsurface S-wave velocity model has been developed. We simulate the MHV curves via the SHV. Then, we attempt to analyze the features of the SHV curves with changes in the *R/L* values. We also study the sensitivity of the SHV curve to verify the feasibility of using the SHV curves to invert the subsurface S-wave velocity structure.

## Methods

Harkrider (1964) proposed the vertical and horizontal powers of the high-mode surface waves based on the surface wave propagation theory in a layered half-space. Then, assuming that the point sources are randomly distributed, the vertical and horizontal powers of all point sources are integrated to obtain the vertical and horizontal powers of multi-order surface waves (Harkrider 1964).

Arai and Tokimatsu (2000) indicated that the equation for SHV and *R/L* can be expressed as

$$\mathrm{SHV}(\omega) = \sqrt{\frac{P_{\mathrm{HS}}(\omega)}{P_{\mathrm{VS}}(\omega)}} = \sqrt{\frac{P_{\mathrm{HR}}(\omega) + P_{\mathrm{HL}}(\omega)}{P_{\mathrm{VR}}(\omega)}} \quad (1)$$

$$(R/L)(\omega) = \sqrt{\frac{P_{\mathrm{HR}}(\omega)}{P_{\mathrm{HL}}(\omega)}} \quad (2)$$

where the subscripts *R*, *L*, and *S* indicate Rayleigh, Love, and surface waves, respectively, and $P_{\mathrm{HR}}(\omega)$ and $P_{\mathrm{VR}}(\omega)$ are the horizontal and vertical powers of all mode Rayleigh wave from all point sources at a frequency ω, respectively. These powers can be expressed as

$$P_{\mathrm{HR}}(\omega) = \kappa L_v^2 \sum_{m=0}^{M} \left(\frac{A_{Rm}}{k_{Rm}}\right)^2 \left(\frac{\dot{u}}{\dot{w}}\right)_m^2 \left[1 + \left(\frac{\alpha^2}{2}\right)\left(\frac{\dot{u}}{\dot{w}}\right)_m^2\right] \quad (3)$$

$$P_{\mathrm{VR}}(\omega) = \kappa L_v^2 \sum_{m=0}^{M} \left(\frac{A_{Rm}}{k_{Rm}}\right)^2 \left[1 + \left(\frac{\alpha^2}{2}\right)\left(\frac{\dot{u}}{\dot{w}}\right)_m^2\right] \quad (4)$$

where *A* is the medium response factor (Harkrider 1964, 1970); m and *M* indicate surface modes; *k* is the wave number; $\dot{u}/\dot{w}$ is the H/V ratio of Rayleigh wave velocity on free surface (Haskell 1953); $L_V$ is the vertical loading force of a microtremor; $\kappa = (2/h)e^{-4\pi h}$, *h* is the scattering damping ratio of soil; α is the H/V ratio of microtremor loading sources, and $\alpha = L_H/L_V$, and $P_{\mathrm{HL}}(\omega)$ is the horizontal power of all mode Love waves from all point sources at a frequency ω. This power can be expressed as

$$P_{\mathrm{HL}}(\omega) = \kappa L_v^2 \sum_{m=0}^{M} \left(\frac{\alpha^2}{2}\right)\left(\frac{A_{Lm}}{k_{Lm}}\right)^2. \quad (5)$$

## Simulation of microtremor H/V spectral curves

### Soil structure parameters and H/V spectral curves of microtremors

The Yuxi basin shown in Fig. 1 is located in the southern end of the fault zone, and it is a typical sedimentary basin in southwestern China. Yuxi City is located in the southeastern part of the basin, and site B is closer to the city, while site A is far from the city. The S-wave velocity profiles are shown in Fig. 2 at sites A and B. Moreover, He et al. (2013) estimated the subsurface velocity structures of the Yuxi basin from the results of seismic exploration. The velocity structures below the depth of the borehole can be obtained from this velocity model (Table 1). The bedrock depths of sites A and B are 415 and 189 m, respectively.

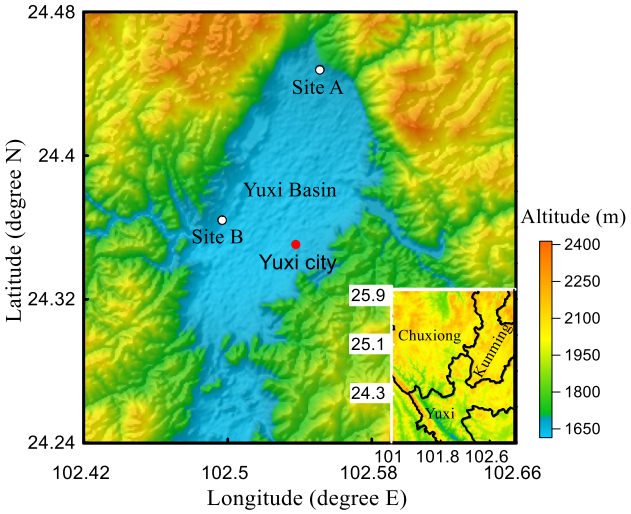


**Fig. 1** Location/map of the Yuxi basin. The white dots represent single-station three-component microtremor observation sites. The red dot represents Yuxi City. The color scale bar shows the altitude

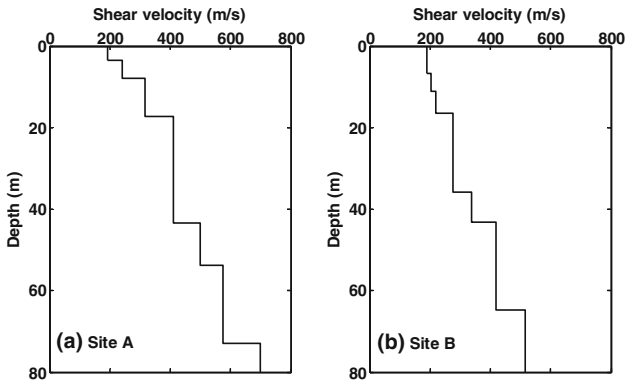


**Fig. 2** Shallow subsurface S-wave velocity profile obtained from boreholes at sites A and B

**Table 1** Velocity structures below the depth of the borehole based on the results of seismic exploration near site A

| Depth (m) | $V_S$ (m/s) | $V_P$ (m/s) | ρ (t/m$^3$) |
|---|---|---|---|
| 80–100 | 700 | 1534 | 1.9 |
| 100–185 | 800 | 1720 | 2.1 |
| 185–415 | 1200 | 2433 | 2.2 |
| 415–900 | 1700 | 2766 | 2.4 |
| > 900 | 3000 | 5326 | 2.5 |

Microtremor signals are recorded by a single-station three-component seismometer with a sampling frequency of 8 ms at sites A and B. On June 3, 2012 at 14:26, 14:34, and 14:43, three sections of microtremors were recorded at site A. On May 27, 2012 at 18:02, 18:16, and 18:26, three sections of microtremors were recorded at site B. Each

section of microtremor is 360.448 s. For each section of microtremor, 16.384 s at the head and the end each is removed, because these records contain interference by human factors. To reduce the measurement error, ten sets of data segments of 32.768 s each are used from each section of the microtremors. Hence, at each site, microtremor records of 983.04 s (30 sets of data segments) are used for the calculation of MHV curves. The MHV at frequency ω is defined as

$$\mathrm{MHV}(\omega) = \sqrt{\frac{P_{\mathrm{EW}}(\omega) + P_{\mathrm{NS}}(\omega)}{P_{\mathrm{UD}}(\omega)}} \tag{6}$$

where $P_{\mathrm{EW}}$ and $P_{\mathrm{NS}}$ are the Fourier power spectra of the two orthogonal horizontal motions and $P_{\mathrm{UD}}$ is the Fourier power spectrum of the vertical motion.

## Measured H/V and simulated H/V curves

To calculate the SHV using Eq. 1, α values are required. The α values can be determined from Eq. 2, because the *R/L* values can be evaluated by microtremor array data. The relative proportion of Love waves in the horizontal components of microtremors varies widely (from 60 to 90%) with the frequency (Köhler et al. 2007; Endrun 2011). Arai and Tokimatsu (2000) indicated that the *R/L* values vary between 0.4 and 1.0 and have an average of approximately 0.7, with a period in the range of 0.1–5 s. We calculated the MHV and SHV curves for *R/L* values of 0.4, 0.7, and 1.0, and they are shown in Fig. 3. In the figure, the MHV curves are between the maximum and minimum curves of the SHV. Hence, a reasonable assumption is that the *R/L* values are in the range of 0.4–1.0 at those sites and frequencies.

The microtremor H/V curve can be used to evaluate the site effect and the subsurface velocity structures. The fundamental resonance frequency of the site is the key to evaluating the site effect and the subsurface velocity profile. The frequency window selected for the analysis of microtremors must contain the fundamental resonance frequency of the site (Picozzi et al. 2005; Sánchez-Sesma et al. 2011). The fundamental resonance frequencies of sites A and B are estimated to be 0.55 and 1.5 Hz, respectively. Accordingly, at sites A and B, we chose the H/V spectral curve in a frequency range of 0.1–5 Hz to analyze the features of SHV curves. Because the bedrock depth of site B (189 m) is less than the bedrock depth of site A (402 m), the fundamental resonance frequency of site B is greater than that of site A, as shown in Fig. 3.

The amplitude of the SHV curve decreases as the *R/L* value increases, as shown in Fig. 3. The amplitude deviation between the MHV and SHV curves for *R/L* value of *n* at the frequency ω can be expressed as

$$D_n(\omega) = |\mathrm{MHV}(\omega) - \mathrm{SHV_n}(\omega)| \tag{7}$$

where *n* is the *R/L* value (*n* in a range from 0.4 to 1.0). The amplitude deviation between the SHV for *R/L* values of 0.4 and the SHV for *R/L* values of 1.0 is 4.44 at the peak frequency (0.5 Hz) at site A, and the amplitude deviations decrease gradually from 4.44 as distance from the peak frequency increases. The amplitude deviation between the SHV for *R/L* values of 0.4 and the SHV for *R/L* values of 1.0 is 2.39 at the peak frequency (1.4 Hz) at site B, and the amplitude deviations decrease gradually from 2.39 as the distance from the peak frequency increases. These findings suggest that the SHV curves are most sensitive to *R/L* values at the peak frequencies of the spectrum and the

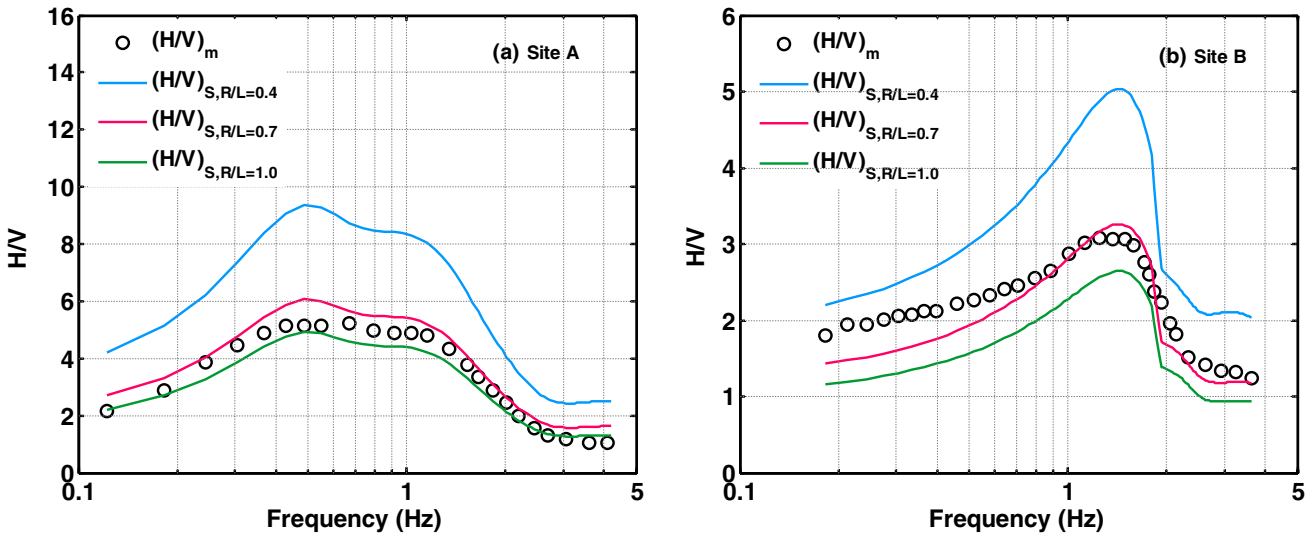


**Fig. 3** Comparison of the measured H/V (open circles) with the simulated H/V (solid lines) obtained using a 1-D velocity structure model at sites A and B. The blue line, red line, and green line represent the H/V of surface waves for *R/L* values of 0.4, 0.7, and 1.0, respectively

sensitivity of the SHV curves to the *R/L* values decreases as the distance from the peak frequency increases.

To obtain more general results, we used two different soil models (a normal soil model and a low-velocity soil model) and calculated the SHV obtained using a 1-D velocity structure model (Fig. 4). We can reach the same conclusion from Fig. 4, in which the SHV curves are most sensitive to *R/L* values at the peak frequencies of the spectrum. Therefore, when the MHV curves are simulated by the SHV curves, where the *R/L* value is constant, the amplitude deviation between the MHV and SHV curves at the near-peak frequency is higher, as shown in Fig. 3. The degree of fitting between the SHV and MHV curves directly affects the accuracy of the velocity structures obtained by the inversion of the microtremor H/V spectrum. To reduce the error of the subsurface velocity structures obtained by the MHV curves, we suggest that the SHV curves at the near-peak frequencies should not be considered in the inversion of the microtremor H/V spectrum, because the amplitude deviation between the MHV and SHV curves is higher at the peak frequency of the MHV curves.

The peak frequencies of the SHV curves for *R/L* values of 0.4, 0.7, and 1.0 are similar to those of the MHV curves, although the amplitudes are not exactly consistent. Therefore, the peak frequencies of the SHV curves are independent of the *R/L* values and are not affected by the α value in the area studied. The amplitude of SHV for the constant *R/L* value is not consistent with that of the MHV curves, because the *R/L* value varies widely based on the site conditions and frequencies.

Figure 5 shows the amplitude deviations between the MHV and SHV curves for different *R/L* values and frequencies at sites A and B obtained using Eq. 7. The range of best *R/L* values at site B is larger than that at site A, as shown in Fig. 5. The fluctuations of the best *R/L* values in the high-frequency part (> 1 Hz) of the MHV curve are significantly higher than those in the low-frequency part (< 1 Hz) at site B, which is likely because the high-frequency part (> 1 Hz) of microtremor signal is primarily influenced by artificial noise (Seht and Wohlenberg 1999). These microtremor signals are recorded during the day, and site B is located close to the city. Human activities cause the points to fluctuate in a larger range at site B. As a result, the fluctuation range of the best *R/L* values is significantly larger in the high-frequency range.

When the *R/L* values are estimated by analyzing the spatial autocorrelation function of the microtremor array records, the *D* values are less than 0.2 (Arai and Tokimatsu 2000). Moreover, the inversion results of the MHV curves can ensure that the *D* values are less than 0.2 (Parolai et al. 2005; Picozzi et al. 2005). We define the best *R/L* value as the value that generates amplitude deviations between the SHV and MHV curves (*D* values) that are less than 0.2. We use the best *R/V* values obtained from Fig. 5 to simulate the MHV curves. When the *R/L* value is the best, the SHV curves simulate MHV curves very well, as shown in Fig. 6. We approximate the best *R/L* values as the true *R/L* values.

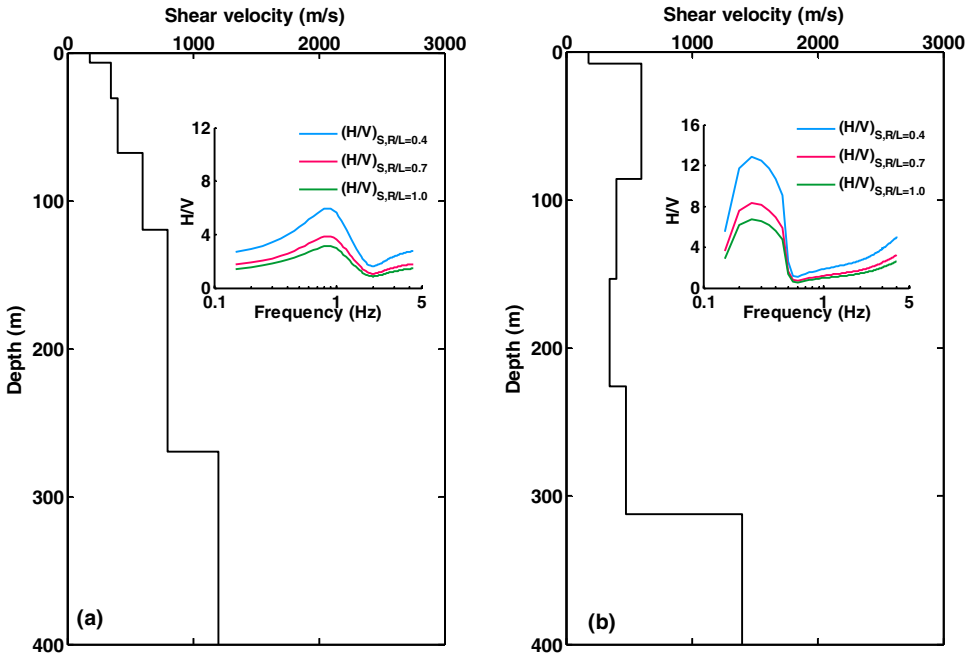


**Fig. 4** S-wave velocity profile and H/V spectra of surface waves (solid lines) obtained using a 1-D velocity structure model with two different hypothetical models. The blue line, red line, and green line represent the H/V of surface waves when the *R/L* values are 0.4, 0.7, and 1.0, respectively

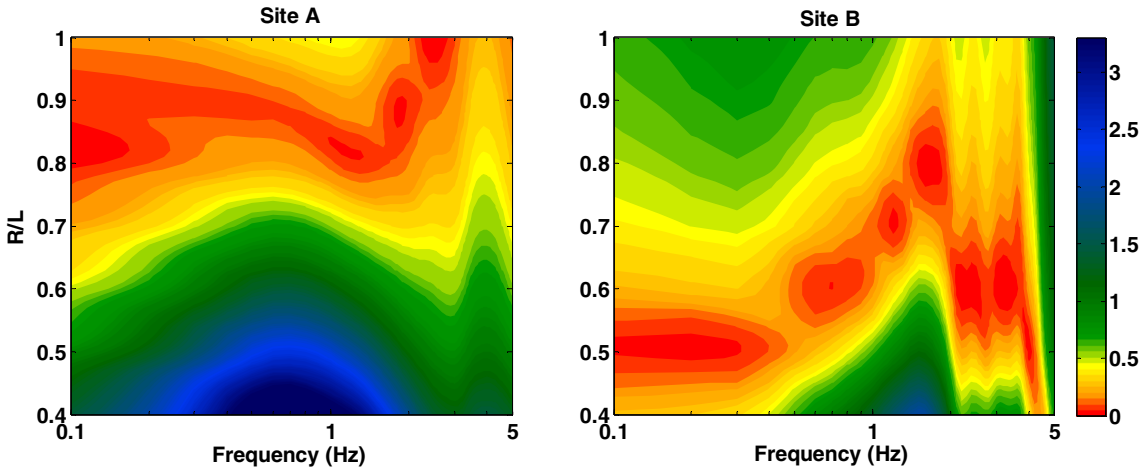


**Fig. 5** Amplitude deviations between the MHV and SHV curves for different *R/L* values and frequencies at sites A and B obtained using Eq. 7. The color scale bar shows the amplitude deviations between the MHV and SHV curves

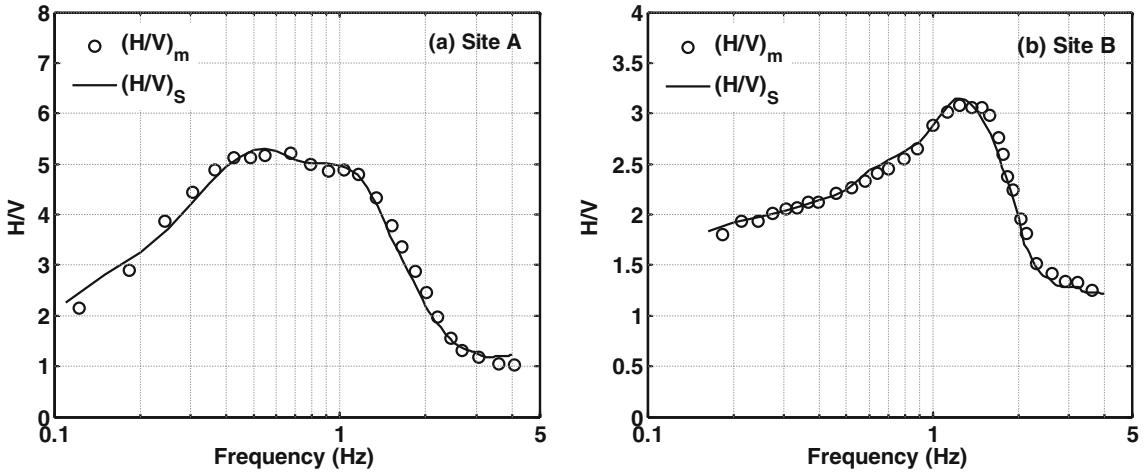


**Fig. 6** Comparison of the measured H/V (open circles) with the simulated H/V (solid lines) of the best *R/L* values at sites A and B

## Sensitivity analysis of the surface wave H/V spectrum

To verify the feasibility of using MHV curves to estimate subsurface velocity structures, the sensitivities of the SHV curves must be analyzed. The sensitivities of the SHV curves (Arai and Tokimatsu 2000), which are the absolute values of the dimensionless partial derivative of SHV for any parameter P of the soil models, can be expressed as

$$S_{\mathrm{ji}}^{p}(\omega) = \left| \frac{P}{\mathrm{SHV}(\omega)} \frac{\partial \mathrm{SHV}(\omega)}{\partial P} \right|_{P=P_{ji}} \tag{8}$$

where $S_{ji}^{p}$ is the sensitivity of the SHV and $P_{ji}$ may represent the thickness $H_j$, the P-wave velocity $V_{Pj}$, the S-wave velocity $V_{Sj}$, and the density $\rho_j$ in the $j$th layer of the soil model.

The sensitivities ($S$) of the SHV curves for the soil model parameters at site A that were obtained using Eq. 8 are shown as Fig. 7. The S-wave velocity and thickness of the soil layer have a great influence on the SHV curve, whereas the density and P-wave velocity of the soil layer have a lesser influence on the SHV curve. Therefore, the inversion of MHV curves can be best achieved by adjusting either the S-wave velocity, thickness or both these parameters at each soil layer.

The maximum $S$ values ($S_{\max}$) of the SHV curves for the soil layer parameters in a frequency range of 0.1–5 Hz are shown in Fig. 8. At site A, the $S_{\max}$ values are mainly concentrated in a frequency range of 1.1–2.4 Hz, which is between the peak and trough frequencies of the H/V spectrum of microtremors recorded at site A. At site B, the $S_{\max}$ values are concentrated in a frequency range of 1.4–2.4 Hz, which is between the peak and trough frequencies of the H/V spectrum of microtremors recorded at site B. In addition, Fig. 7 shows that the $S$ values at frequencies less than 1 Hz are far less than those at frequencies greater than

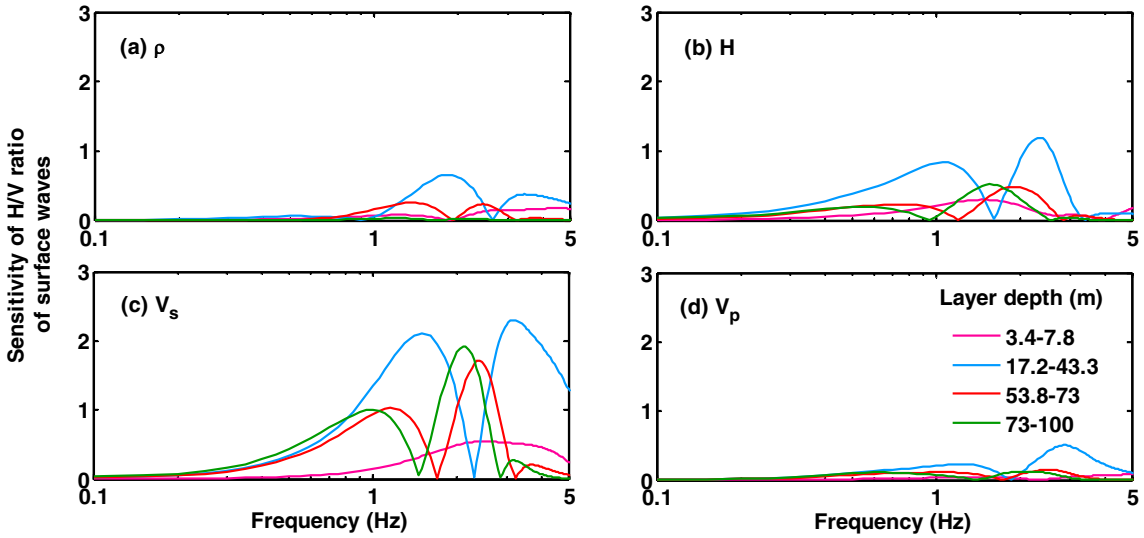


**Fig. 7** Sensitivity value S of the surface wave H/V spectrum for the soil model parameters at site A obtained using Eq. 8. **a–d** *S* Values for the density, thickness, and S- and P-wave velocity of the soil layers

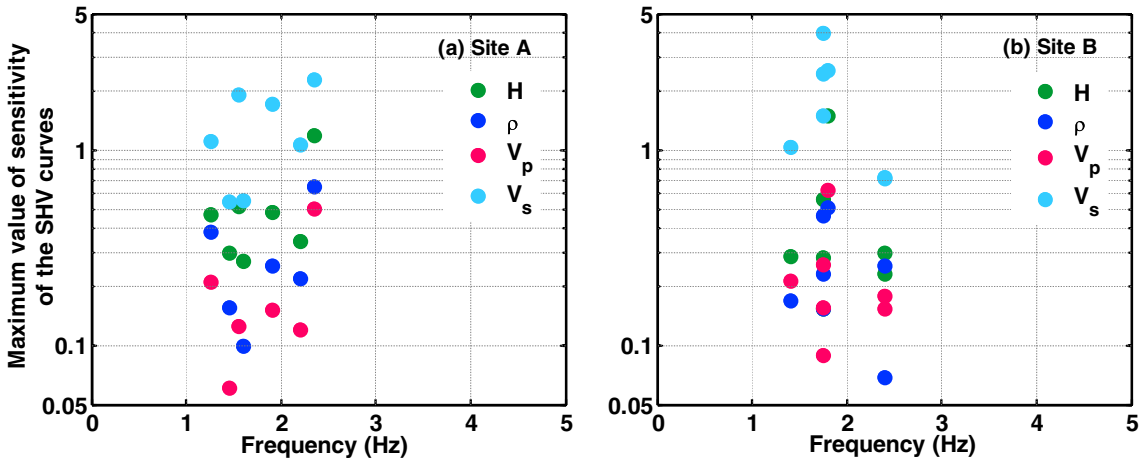


**Fig. 8** Maximum sensitivity value of the SHV curves for shallow soil model parameters

1 Hz at site A. The same trends can be obtained from the soil model at site B. Therefore, the spectrum curves are sensitive to the parameters in a frequency range that is located between the peak and trough frequencies of the microtremor H/V spectrum. Therefore, this frequency range is the most suitable for inversion.

## Discussion

We simulated MHV curves using the surface wave propagation theory in a layered half-space. In Fig. 3, we compare the MHV and SHV for *R/L* values of 0.4, 0.7 and 1. The misfit is clearly different for both *R/L* curves compared to the measured H/V. In this paper, we find the best *R/L* values by simulating MHV curves for different values and by evaluating the misfit with respect to the measured MHV. Figure 5 shows that the best *R/L* values are stable in the range of 0.8–1.0 with changes in frequency at site A, and the best *R/L* values are stable in the range of 0.4–0.9 with changes in frequency at site B. Hence, the *R/L* values vary widely based on the site condition and frequency. Bonnefoy-Claudet et al. (2008) and Endrun (2011) calculated *R/L* values via a frequency-dependent analysis of the main propagation and polarization based on microtremor array measurements and found that the relative proportion of Love and Rayleigh waves in the microtremors varies widely with frequency and site conditions and the *R/L* values are stable in the ranges of 0.2–1.0. At sites A and B, the best *R/L* values we get are also in this range. However, the *R/L* value cannot be evaluated from microtremor data recorded by a single-station three-component seismometer

if the velocity model is unknown. Further study is required to determine a method of identifying the true *R/L* values to estimate the subsurface velocity structure using the H/V spectrum of microtremors recorded by a single-station three-component seismometer.

Figures 3 and 4 show that the SHV curves are the most sensitive to *R/L* values at the peak frequencies of the spectrum. To reduce the error of subsurface velocity structures obtained from the MHV curves, the SHV curves at the near-peak frequencies should not be considered in the inversion of the microtremor H/V spectrum. Because the location of the peak frequency depends on the subsurface structure, it varies naturally from low to high frequencies for different sites. Therefore, we cannot provide a specific frequency range that contains the peak frequency that is not used to estimate the velocity structures.

Finally, we analyze the sensitivity of the SHV curves. Figure 7 confirms that the S-wave velocity and the thickness of the soil layer has a great influence on the SHV curve. By calculating the partial derivatives of the H/V spectrum of Rayleigh waves, Tsuboi and Saito (1983) indicated that the H/V curves are most sensitive to the S-wave velocity. Furthermore, the MHV curves are sensitive to the parameter in a frequency range that is located between the peak and trough frequencies of the SHV, as shown in Fig. 7. In the process of applying the mode summation method and a finite difference technique to investigate the spectral ratio, Fäh et al. (2001) similarly found that the MHV curves are controlled by the ellipticity of the fundamental-mode Rayleigh wave in the frequency band between the fundamental frequency of resonance of the sediments and the first minimum of the average H/V ratio. Although the peak frequencies of the H/V spectral ratio of fundamental-mode Rayleigh waves are similar to that of the microtremors in general, there are some sites with a low impedance contrast, where the Love waves dominate the wavefield at the H/V peak. Hence, a more reasonable approach is to express the sensitive frequency range of MHV using surface waves rather than Rayleigh waves.

## Conclusions

In this study, we used the SHV equation based on the surface wave propagation theory in a layered half-space to simulate the MHV curves of sites A and B in the Yuxi basin. We found that the peak frequency of the SHV curve is independent of the α value, although the amplitude of the SHV curve has some relation with the α value. Furthermore, we found that the SHV curves are most sensitive to *R/L* values at the peak frequencies of the spectrum. Therefore, to reduce the error of subsurface velocity structures obtained by the MHV curves, we suggest that the SHV curves at the near-peak frequencies should not be considered in the inversion of the microtremor H/V spectrum, because the amplitude deviation between the MHV and SHV curves is higher at the peak frequency of the MHV curves.

In addition, to verify the feasibility of the inversion of MHV curves, we analyzed the features of the sensitivity of SHV curves. We confirmed that the inversion of MHV curves can be best achieved by adjusting either the S-wave velocity, thickness, or both these parameters at each soil layer. Moreover, the best frequency range for the inversion of the microtremor H/V spectrum is between the peak and trough frequencies of the microtremor H/V spectrum.

**Acknowledgements** This research work was supported by the National Natural Science Foundation of China (Nos. 51278470, 51678537) and the Key Laboratory of Seismic Observation and Geophysical Imaging Project. The microtremor records were obtained from the China Seismic Array at http://www.chinaarray.org. The authors thank the anonymous referees for their comments, which contributed to improving the work.

## Compliance with ethical standards

**Conflict of interest** On behalf of all authors, the corresponding author states that there are no conflicts of interest.

## References

Aki K (1957) Space and time spectra of stationary stochastic waves, with special reference to microtremors. Bull Earthq Res Inst Tokyo Univ 35:415–456

Apostolidis P, Raptakis D, Roumelioti Z, Pitilakis K (2004) Determination of S-wave velocity structure using microtremors and SPAC method applied in Thessaloniki (Greece). Soil Dyn Earthq Eng 24(1):49–67. https://doi.org/10.1016/j.soildyn.2003.09.001

Arai H, Tokimatsu K (2000) Effects of Rayleigh and Love waves on microtremor H/V spectra. In: the 12th world conference on earthquake engineering, Auckland, New Zealand, 30 January–4 February 2000

Arai H, Tokimatsu K (2004) S-wave velocity profiling by inversion of microtremor H/V spectrum. Bull Seismol Soc Am 94(1):53–63

Arai H, Tokimatsu K (2005) S-wave velocity profiling by joint inversion of microtremor dispersion curve and horizontal-to-vertical (H/V) spectrum. Bull Seismol Soc Am 95(5):1766–1778. https://doi.org/10.1785/0120040243

Bonnefoy-Claudet S, Cornou C, Bard PY, Cotton F, Moczo P, Kristek J, Fäh D (2006) H/V ratio: a tool for site effects evaluation. Results from 1-D noise simulations. Geophys J Int 167(2):827–837

Bonnefoy-Claudet S, Köhler A, Cornou C, Wathelet M, Bard PY (2008) Effects of Love waves on microtremor H/V ratio. Bull Seismol Soc Am 98(1):288–300

Capon J (1969) High-resolution frequency-wavenumber spectrum analysis. Proc IEEE 57(8):1408–1418

Carcione JM, Picotti S, Francese R, Giorgi M, Pettenati F (2017) Effect of soil and bedrock anelasticity on the S-wave amplification function. Geophys J Int 208:424–431

Chen XL, Gao MT, Yu YX, Chen K, Li TF (2014) Applicability of topographic slope method for seismic site soil classification of Yuxi-Jiangchuan-Tonghai-Basin in China. Earthq Eng Eng Dyn S1:146–152 **(in Chinese)**

Claprood M, Asten MW, Kristek J (2011) Using the SPAC microtremor method to identify 2D effects and evaluate 1D shear-wave velocity profile in valleys. Bull Seismol Soc Am 101 (101):826–847. https://doi.org/10.1785/0120090232

Delgado J, Casado CL, Giner J, Estevez A, Cuenca A, Molina S (2000) Microtremors as a geophysical exploration tool: applications and limitations. Pure Appl Geophys 157(9):1445–1462

Dolenc D (2005) Microseisms observations in the Santa Clara Valley, California. Bull Seismol Soc Am 95(3):1137–1149

Endrun B (2011) Love wave contribution to the ambient vibration H/V amplitude peak observed with array measurements. J Seismol 15(3):443–472

Fäh D, Kind F, Giardini D (2001) A theoretical investigation of average H/V ratios. Geophys J Int 145(2):535–549

Fäh D, Kind F, Giardini D (2003) Inversion of local s-wave velocity structures from average H/V ratios, and their use for the estimation of site-effects. J Seismol 7(4):449–467. https://doi.org/10.1023/B:JOSE.0000005712.86058.42

Gao MT, Yu YX, Zhang XM, Wu J, Hu P, Ding YH (2002) Three-dimensional finite-difference simulations of ground motions in the Beijing area. Earthq Res China 18(4):356–364 **(in Chinese)**

García-Jerez A, Luzón F, Sánchez-Sesma FJ, Lunedei E, Albarello D, Santoyo MA, Almendros J (2013) Diffuse elastic wavefield within a simple crustal model. Some consequences for low and high frequencies. J Geophys Res-Solid Earth 118(10):5577–5595

García-Jerez A, Piña-Flores J, Sánchez-Sesma FJ, Luzón F, Perton M (2016) A computer code for forward calculation and inversion of the H/V spectral ratio under the diffuse field assumption. Comput Geosci 97:67–78

Guéguen P, Cornou C, Garambois S, Banton J (2007) On the limitation of the h/v spectral ratio using seismic noise as an exploration tool: application to the grenoble valley (france), a small apex ratio basin. Pure Appl Geophys 164(1):115–134. https://doi.org/10.1007/s00024-006-0151-x

Harkrider DG (1964) Surface waves in multilayered elastic media, part 1. Bull Seismol Soc Am 54(2):627–679

Harkrider DG (1970) Surface waves in multilayered elastic media, part 2. Bull Seismol Soc Am 60(6):1937–1987

Haskell NA (1953) The dispersion of surface waves on multilayered media. Bull Seismol Soc Am 43(1):17–34

He ZQ, An HS, Shen K, Lu LY, Hu G, Ye TL (2013) Detection of Puduhe fault in Yuxi basin of Yunnan by seismic reflection method. Acta Seismol Sin 35(6):836–847 **(in Chinese)**

Hobiger M, Bard PY, Cornou C, Bihan NL (2009) Single station determination of Rayleigh wave ellipticity by using the random decrement technique (RayDec). Geophys Res Lett 36(14): L14303

Horike M (1985) Inversion of phase velocity of long-period microtremors to the S-wave-velocity structure down to the basement in urbanized areas. J Phys Earth 33(2):59–96

Köhler A, Ohrnberger, M., Scherbaum, F (2006) The relative fraction of Rayleigh and Love waves in ambient vibration wavefields at different European sites. In: Third international symposium on the effects of surface geology on seismic motion Grenoble, France, 30 August–1 September 2006

Köhler A, Ohrnberger M, Scherbaum F, Wathelet M, Cornou C (2007) Assessing the reliability of the modified three-component spatial autocorrelation technique. Geophys J Int 168(2):779–796

Komatitsch D, Liu Q, Tromp J, Süss P, Stidham C, Shaw JH (2004) Simulations of ground motion in the Los Angeles basin based upon the spectral-element method. Bull Seismol Soc Am 94 (1):187–206

Lachetl C, Bard PY (1994) Numerical and theoretical investigations on the possibilities and limitations of Nakamura's technique. Earth Planets Space 42(5):377–397. https://doi.org/10.4294/jpe1952.42.377

Lunedei E, Albarello D (2010) Theoretical HVSR curves from full wavefield modelling of ambient vibrations in a weakly dissipative layered Earth. Geophys J Int 181(2):1342–1342

Lunedei E, Malischewsky P (2015) A review and some new issues on the theory of the H/V technique for ambient vibrations. Perspectives on european earthquake engineering and seismology. Springer, New York, pp 371–394

Malischewsky PG, Scherbaum F (2004) Love's formula and H/V-ratio (ellipticity) of Rayleigh waves. Wave Motion 40:57–67

Nogoshi M, Igarashi T (1971) On the amplitude characteristics of microtremor (part 2). J Seismol Soc Jpn 24(1):26–40

Özalaybey S, Zor E, Ergintav S, Tapırdamaz MC (2011) Investigation of 3-d basin structures in the İzmit bay area (turkey) by single-station microtremor and gravimetric methods. Geophys J Int 186 (2):883–894

Parolai S, Picozzi M, Richwalski SM, Milkereit C (2005) Joint inversion of phase velocity dispersion and H/V ratio curves from seismic noise recordings using a genetic algorithm, considering higher modes. Geophys Res Lett 32(1):67–100. https://doi.org/10.1029/2004GL021115

Picozzi M, Parolai S, Richwalski SM (2005) Joint inversion of H/V ratios and dispersion curves from seismic noise: estimating the S-wave velocity of bedrock. Geophys Res Lett 32(11):339–357. https://doi.org/10.1029/2005GL022878

Piña-Flores J, Perton M, Garcíajerez A, Carmona E, Luzon F, Molina-Villegas JC, S´anchez-Sesma FJ (2017) The inversion of spectral ratio H/V in a layered system using the diffuse field assumption. Geophys J Int 208:577–588

Rhie J, Dreger D (2009) A simple method for simulating microseism H/V spectral ratio in 3D structure. Geosci J 13(4):401–406. https://doi.org/10.1007/s12303-009-0036-y

Rong MS, Wang ZM, Woolery EW, Lyu YJ, Li XJ, Li SY (2016) Nonlinear site response from the strong ground-motion recordings in western China. Soil Dyn Earthq Eng 82(4):99–110

Sánchez-Sesma FJ, Rodríguez M, Iturrarán-Viveros U, Luzón F, Campillo M, Margerin L, García-Jerez A, Suarez M, Santoyo MA, Rodríguez-Castellanos A (2011) A theory for microtremor H/V spectral ratio: application for a layered medium. Geophys J Int 186(1):221–225. https://doi.org/10.1111/j.1365-246X.2011.05064.x

Satoh T, Kawase H, Iwata T, Higashi S, Sato T, Irikura K, Huang HC (2001) S-wave velocity structure of the Taichung basin, Taiwan, estimated from array and single-station records of microtremors. Bull Seismol Soc Am 91(5):1267–1282

Seht IV, Wohlenberg J (1999) Microtremor measurements used to map thickness of soft sediments. Bull Seismol Soc Am 89 (1):250–259

Shani-Kadmiel S, Tsesarsky M, Louie JN, Gvirtzman Z (2012) Simulation of seismic-wave propagation through geometrically complex basins: the dead sea basin. Bull Seismol Soc Am 102 (4):1729–1739

Tamura S (1996) Comparison of body and Rayleigh wave displacements generated by a vertical point force on a layered elastic medium. In the 11th World conference on earthquake engineering, Acapulco, Mexico, 23–28 June 1996

Tsuboi S, Saito M (1983) Partial derivatives of Rayleigh wave particle motion. Earth Planets Space 31(2):103–113

Uebayashi H (2003) Extrapolation of irregular subsurface structures using the horizontal-to-vertical spectral ratio of long-period microtremors. Bull Seismol Soc Am 93(2):570–582

Uebayashi H, Kawabe H, Kamae K (2012) Reproduction of microseism H/V spectral features using a three-dimensional

complex topographical model of the sediment-bedrock, interface in the Osaka sedimentary basin. Geophys J Int 189(2):1060–1074. https://doi.org/10.1111/j.1365-246X.2012.05408.x

Wu CF, Huang HC (2012) Estimation of shallow S -wave velocity structure in the Puli basin, Taiwan, using array measurements of microtremors. Earth Planets Space 64(5):389–403. https://doi.org/10.5047/eps.2011.12.002

Yamanaka H, Takemura M, Ishida H, Niwa M (1994) Characteristics of long-period microtremors and their applicability in exploration of deep sedimentary layers. Bull Seismol Soc Am 84 (6):1831–1841